Thermo-Acoustic Growth Rate Determination from Numerical and Experimental Data for Rocket Engine Applications

By A. Chemnitz, N. Kings, T. Sattelmayer†
N. Blanco, J. Hardi, M. Oschwald‡
E. Boujo, G. Bonciolini AND N. Noiray¶

The thermoacoustic stability behavior of a rocket engine, i.e. the interaction of combustor acoustics and heat release, is characterized by the damping or growth rates describing the temporal development of the chamber pressure when displaced from its equilibrium value. This report tackles the computation of this quantity from experimental and numerical data. The test case under consideration is a multi-injector H_2/O_2 rocket combustion chamber, showing an instability of the 1st transverse mode at certain load points. The numerical modeling is based on the Linearized Euler Equations with flame feedback included via a source term. For the calculation of damping rates, Lorentzian and exponential fitting are used along with statistical parameter extraction based on the Fokker-Planck equation. These methods differ in their suitability for signals of different type (stochastic/deterministic) and stability behavior. Together, they cover all the cases studied in this work. The results revealed the applicability of the Fokker-Planck approach to certain experimental load points and provided an assessment of the parameter dependence of the other two extraction methods. Thereby, the Lorentzian fit appears to be more robust regarding the studied influencing factors.

1. Introduction

Ensuring stable operating conditions in the combustion chamber is a crucial issue for the development of rocket engines. The occurrence of an instability, i.e. the back coupling and mutual amplification of chamber acoustics and heat release can ultimately lead to the destruction of the whole engine. The quantitative evaluation of a combustor's damping rate is a key aspect in judging the stability of an engine. The final goal is a set of consistent extraction methods that are tailored to the respective characteristics of numerical and experimental data and allow for a reliable comparison of the obtained damping rates. In a first step, the application of different damping rate calculation methods to suitable numerical and experimental signals has been tested. The initial results are covered in this report.

† Institute of Thermodynamics, Technical University of Munich, Boltzmannstr. 15, 85747 Garching
‡ Institute of Space Propulsion, German Aerospace Center, Im Langen Grund, 74239 Hardthausen
¶ Institute of Energy Technology, Swiss Federal Institute of Technology Zurich, Sonneggstrasse 3, 8092 Zurich

The test case studied is a multi-injector H_2/O_2 combustor, which shows stable or unstable operation, depending on the load point. Focus is placed on the dominant 1st transverse mode. Thereby the different nature of the numerical and experimental signals needs to be accounted for. Particularly, in the experiment an unstable signal quickly reaches a limit-cycle due to non-linear saturation effects, while the numerical simulation base on the Linearized Euler Equations (LEE) and thus predict unlimited growth. Furthermore, turbulence leads to stochastic forcing of the combustor in the experiment. This is not included in the numerical model, which results in deterministic signals. These differences need to be accounted for in the data processing, while at the same time maintaining comparability between the extracted results.
In this work, different damping rate calculation procedures are tested on rocket engine data, giving an overview of the influencing parameter of the respective methods and the current progress regarding their usage for evaluation of transverse combustor modes. The different extraction methods are described in the next section. Then, after an outline of experimental and numerical data generation, the results obtained for these signals are presented and discussed.

2. Damping Rate Extraction Methods

Various approaches are in use to obtain the thermoacoustic growth rates from a signal. In this section, three methods based on Lorentzian fit, exponential fit and Fokker-Planck equation, are introduced. The applicability of the different methods depends on several aspects. First, the nature of the signal is of relevance. As outline before, the numeric approach used in this work produces deterministic signals with unlimited growth for the unstable cases. In contrast, the experimentally recorded pressure gives a statistical signal and approaches a limit cycle with comparatively small deviations of the pressure from the corresponding equilibrium value. Thus, the evaluation of damping rates needs to be based on transient signals for the numerical as opposed to limit cycle conditions for the experimental case. The second factor to be considered is the stability behavior. The widely used Lorentzian fit is applicable to decaying oscillations only, limiting its use to the evaluation of stable load points. In contrast, the Fokker-Planck and exponential fitting methods are appropriate for both, stable and unstable conditions. The respective methods are outlined in the following.

2.1. *Lorentzian Fitting*

The Power Spectral Density (PSD) of a damped harmonic oscillation possesses a characteristic shape, which is most significant at the frequencies neighboring the oscillation frequency. This profile corresponds to a Lorentzian curve, described via the equation [1]

$$PSD \propto \frac{1}{(\omega - \omega_0)^2 + \alpha_D^2} \quad . \tag{2.1}$$

The damping rate α_D corresponds to the curve's half width at half maximum. It can be obtained by fitting the Lorentzian curve to the PSD of the signal. However, this approach is only applicable to stable load points.
For the fitting procedure, several aspects have to be taken into account. First, the oscillation frequency ω_0 can be either set fixed, based on the frequency content of the signal, or left as free parameter. The latter has been chosen in this work, since fitting

the eigenfrequency allows to increase the accuracy of the fit. It partly compensates for the limited frequency resolution of the PSD and to deal with the distortion of the signal via noise. Furthermore, the range of the PSD considered for the fitting is of relevance. Particularly eigenmodes located at frequencies close to that of the mode of interest can distort the shape of the PSD via the superposition of their own frequency content.

2.2. *Exponential Fitting*

Damping rate extraction via exponential fitting directly evaluates the temporal development of the pressure signal. Thereto, a short-time Fourier transform is applied: The data are subdivided in subsequent, potentially overlapping windows, each of which a Fourier transform is taken of. From the resulting spectra, the amplitude at the eigenfrequency of interest is taken and an exponential fit is applied:

$$A = A_0 e^{-\alpha_D t} \quad . \tag{2.2}$$

This method can be used for both, stable and unstable conditions but requires the signal to be transient, i.e. not at limit cycle or decayed. Several parameters can influence the results obtained with this method. Most imminent are overlap and width of the windows. The latter also influences the frequency resolution of the spectrum and thus the accuracy the amplitude can be determined with. Furthermore, a filter can be applied to the data within the single windows.

2.3. *Fokker-Planck Approach*

The stochastic nature of experimental signals and the measurements at limit cycle conditions do not allow for the application of exponential fitting. While Lorentzian fitting is possible for stable load points, a general approach is the system identification using a Fokker-Planck equation. The fundamentals of this approach are outlined in the following, before the actual extraction procedure is described.

2.3.1. *Fundamentals*

We briefly recall the description needed for the system identification; for more details, see [2]. In annular combustors, the acoustic pressure at a given location (fixed axial and radial positions (z, r)) can be written in terms of two fixed orthogonal shape functions and two time-dependent coefficients (modal amplitude):

$$p(t,\theta) = \sum_n \eta_{n,a}(t)\cos(m\theta) + \eta_{n,b}(t)\sin(n\theta) \tag{2.3}$$

where θ is the azimuthal position. If thermoacoustic modes have well separated frequencies, one can focus on one mode at a time. In particular, if one mode is dominant:

$$p(t,\theta) \simeq \eta_{n,a}(t)\cos(n\theta) + \eta_{n,b}(t)\sin(n\theta). \tag{2.4}$$

In the following we consider $n = 1$, which corresponds to the 1st transverse mode.
Inserting this decomposition into the wave equation, considering linear acoustic damping α, using a simple model of flame response (linear and cubic heat release rate response to acoustic forcing, $Q = \beta p - \kappa p^3$), and accounting for turbulence-induced forcing with stochastic terms $\xi(t)$, one obtains a set of second-order stochastic differential

equations for the two oscillators:

$$\ddot{\eta}_a + \omega_n^2 \eta_a = (\beta - \alpha)\dot{\eta}_a - \frac{3\kappa}{4}\left(\dot{\eta}_a(3\eta_a^2 + \eta_b^2) + 2\dot{\eta}_b \eta_a \eta_b\right) + \xi_a, \tag{2.5}$$

$$\ddot{\eta}_b + \omega_n^2 \eta_b = (\beta - \alpha)\dot{\eta}_b - \frac{3\kappa}{4}\left(\dot{\eta}_b(3\eta_b^2 + \eta_a^2) + 2\dot{\eta}_a \eta_b \eta_a\right) + \xi_b, \tag{2.6}$$

where the ξ_i are independent white noise sources of intensity Γ_i, i.e. $\langle \xi_i(t)\xi_i(t+\tau)\rangle = \Gamma_i \delta(\tau)$. The aim of system identification is to estimate the system parameters: linear growth rate $\nu = -\alpha_D = (\beta - \alpha)/2$, nonlinear saturation term κ and noise intensities Γ_i. It is convenient to express the modal amplitudes as:

$$\eta_a(t) = A(t)\cos(\omega_n t + \varphi_a(t)), \quad \eta_b(t) = B(t)\cos(\omega_n t + \varphi_b(t)). \tag{2.7}$$

Due to the stochastic forcing, the oscillation amplitudes $A(t)$, $B(t)$, and phases $\varphi_a(t)$, $\varphi_b(t)$ are not constant but rather fluctuate in a random fashion. Typical operating conditions are such that (2.5)-(2.6) are close to simple harmonic oscillators, $\ddot{\eta} + \omega_n^2 \eta = 0$. Therefore, the envelopes $A(t)$, $B(t)$ vary slowly compared to the acoustic period $2\pi/\omega_n$. Taking advantage of that and averaging (2.5)-(2.6), one obtains a set of three first-order stochastic differential equations for the envelopes $A(t)$, $B(t)$ and the phase difference $\phi(t) = \varphi_a - \varphi_b$. This if further reduced to two equations by using the change of variable $\check{A} = A\sqrt{2 + \cos(2\phi)}$ and $\check{B} = B\sqrt{2 + \cos(2\phi)}$:

$$\dot{A} = \overbrace{\nu A - \frac{3\kappa}{32}(3A^2 + \check{B}^2)A + \frac{\Gamma_a}{4\omega_n^2 A}}^{D_A^{(1)}} + \zeta_a(t), \tag{2.8}$$

$$\dot{B} = \underbrace{\nu B - \frac{3\kappa}{32}(3B^2 + \check{A}^2)B + \frac{\Gamma_b}{4\omega_n^2 B}}_{D_B^{(1)}} + \zeta_b(t), \tag{2.9}$$

where the ζ_i are independent white noise sources of intensity $\Gamma_i/2\omega_n^2$.

Figure 1 shows an example of time signals, and corresponding spectra. The fast oscillation of the modal amplitudes and the slow fluctuation of the envelopes are clearly visible. Two characteristic regimes are shown in figure 2: mainly standing, when one amplitude is dominant, and mainly rotating, when both amplitudes have the same order of magnitude.

3. Extraction Method

With the Langevin equations (2.8)-(2.9) a Fokker-Planck equation is associated, which governs the evolution of the probability density function (PDF) $P(A, B, t)$. This equation is a convection-diffusion equation whose drift coefficients $D_A^{(1)}$, $D_B^{(1)}$ (defined in (2.8)-(2.9) above) and diffusion coefficients $D_A^{(2)} = \Gamma_a/2\omega_n^2$, $D_B^{(2)} = \Gamma_b/2\omega_n^2$ are also called the first and second Kramers-Moyal (KM) coefficients. They can be estimated from time signals $A(t)$, $B(t)$:

$$D_A^{(k)}(A, \check{B}) = \lim_{\tau \to 0} \frac{1}{k!\tau} \iint (a - A)^k P(\{a, \check{b}\}_{t+\tau} | \{A, \check{B}\}_t)\, \mathrm{d}a\mathrm{d}\check{b}, \quad k = 1, 2, \tag{3.1}$$

where $P(\{a, \check{b}\}_{t+\tau} | \{A, \check{B}\}_t)$ is the conditional transition probability (probability that the state is $\{a, \check{b}\}$ at time $t + \tau$ knowing that it was $\{A, \check{B}\}$ at time t). A similar equation

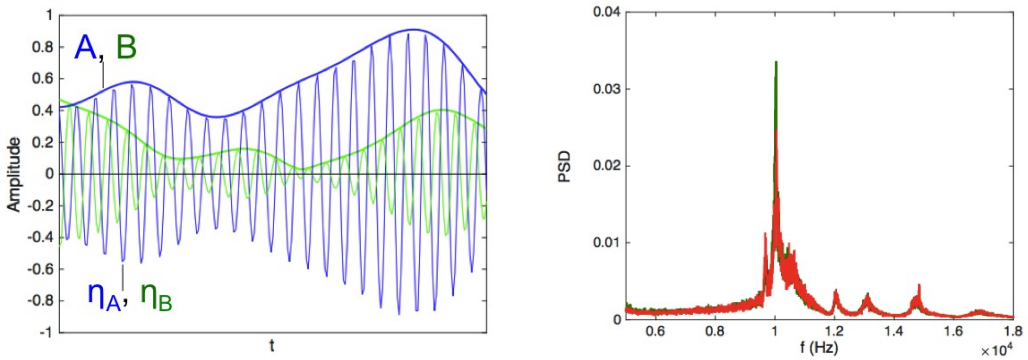

FIGURE 1. Left: time signals of acoustic modal amplitudes $\eta_a(t)$, $\eta_b(t)$ and envelopes $A(t)$, $B(t)$. Right: frequency spectra of $\eta_a(t)$ and $\eta_b(t)$.

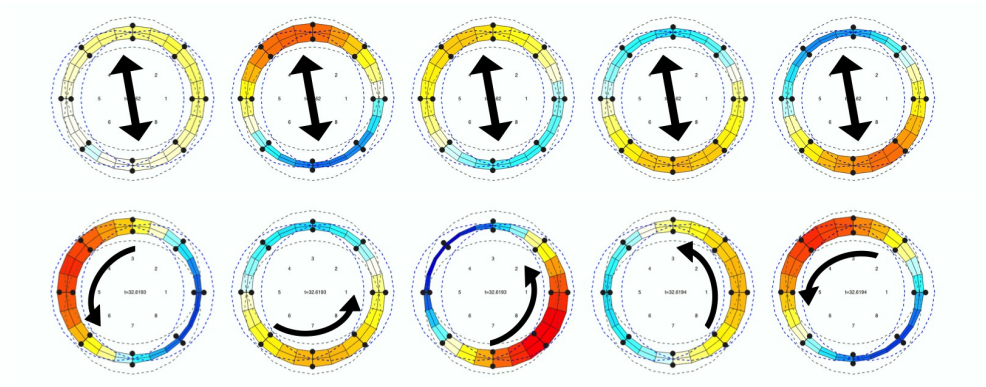

FIGURE 2. Top: standing regime ($A \ll B$). Bottom: rotating regime ($A \simeq B$). Dashed lines: fixed shape functions $\cos(\theta)$, $\sin(\theta)$. Color: acoustic pressure field $\eta_a(t)\cos(\theta) + \eta_b(t)\sin(\theta)$.

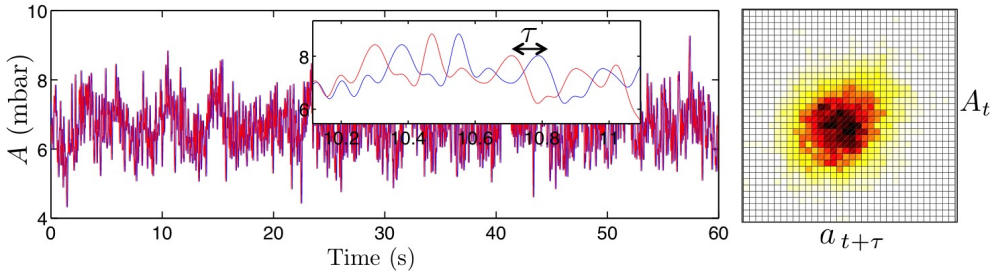

FIGURE 3. Illustration of the parameter identification method: envelopes are time shifted and the conditional transition probability is calculated (here illustrated with $A(t)$ only for simplicity), which allows one to compute the KM coefficients (3.1).

holds for $D_B^{(k)}(\check{A}, B)$. The method is illustrated in figure 3. Comparing the KM coefficients calculated from time series with their analytical expressions, one can identify the parameters ν, κ, Γ_i.

In practice, it is not possible to compute exactly the limit when $\tau \to 0$ and one needs to extrapolate values obtained for finite time shifts τ. If the sampling frequency is not

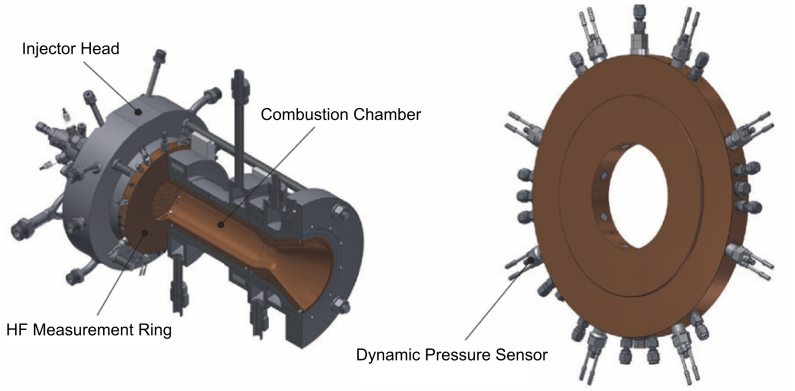

FIGURE 4. BKD test configuration; overview (left) and HF measurement ring (right) [4]

high enough, or if time signals are band-pass filtered to isolate the mode of interest, then this extrapolation is non trivial. The work carried out during this summer program consisted in extending the method proposed in [2], to improve its robustness and accuracy. A new code was developed, with a fast, rigorous and modular implementation. In the ETH code, extrapolation for one mode is conducted accounting for the amplitude distribution of the second mode as well. In contrast, the approach by the DLR carries out the Fokker-Planck analysis for the A mode at a single value of $\breve{B}$ for simplification. There, the modal value is chosen since it has the most data.

4. Evaluation Data

For the damping rate extraction, experimental and numerical data for a LOx/H_2 combustion chamber, termed BKD, are studied. Four load points are considered here, with LP1 and LP3 showing stable operation and LP2 and LP4 being unstable. Details on the load point specifications can be found in [3]. In the following, the experimental setup is introduced, followed by an outline of the numerical approach.

4.1. *Test Case*

The DLR facility at Lampoldshausen, Germany features a test bench where combustion chambers simulating rocket engines can be operated under realistic conditions. Scientific studies of HF instability focus on laboratory scale combustors. BKD is a naturally unstable, cylindrical combustor operating up to 80 bar and features 42 LOx/H2 flames (figure 4 (left)). Access of dynamic pressure sensors is limited to a measurement ring close to the chamber face plate as shown in figure 4 (right) due to high downstream temperatures. The first-tangential (T1) mode of BKD has been identified as the dominant mode at unstable operating points.

4.2. *Numerical Modeling*

Numerically, the development of flow perturbations is calculated via the Linearized Euler Equations (LEE). A quasi one-dimensional mean flow is generated, reproducing the axial development of the averaged sound speed and isentropic compressibility. With this mean flow, the LEE are solved with an enhanced version of the finite difference

code PIANO, originally developed by the DLR and adapted for the current scope of application at the Institute of Thermodynamics, TUM. Flame feedback is accounted for via a source term in the energy equation. The complete set of equations reads:

$$\frac{\partial \rho'}{\partial t} + \overline{u}_i \frac{\partial \rho'}{\partial x_i} + \overline{\rho} \frac{\partial u_i'}{\partial x_i} + \rho' \frac{\partial \overline{u}_i}{\partial x_i} = 0 \tag{4.1}$$

$$\frac{\partial u_i'}{\partial t} + \overline{u}_j \frac{\partial u_i'}{\partial x_j} + \hat{u}_j \frac{\overline{u}_i}{\partial x_j} + \frac{1}{\rho} \frac{\partial p'}{\partial x_i} - \frac{\rho'}{\overline{\rho}^2} \frac{\partial \overline{p}}{\partial x_i} = 0 \tag{4.2}$$

$$\begin{aligned} &\frac{\partial p'}{\partial t} + \overline{u}_i \frac{\partial p'}{\partial x_i} + u_i' \frac{\partial \overline{p}}{\partial x_i} \\ &\quad + \kappa \left(\overline{p} \frac{\partial u_i'}{\partial x_i} + p' \frac{\partial \overline{u}_i}{\partial x_i} \right) - \left(\frac{\overline{p} u_i' + p' \overline{u}_i}{\kappa - 1} \right) \frac{\partial \kappa}{\partial x_i} = (\kappa - 1) \dot{q}' \quad . \end{aligned} \tag{4.3}$$

For the flame feedback, a generic approach is used:

$$\dot{q}' = c_0 \cdot \frac{p'(t - \tau)}{\overline{p}} \quad . \tag{4.4}$$

The value of c_0 ($[c_0] = \frac{W}{m^3}$) has been set constant across the field and the delay time τ has been designed to match the phase of the flame transfer function given in [5] at a frequency of $10000\ Hz$, approximately the frequency of the first transverse mode. This simple flame model has been applied for the unstable LP4, where it provided strong feedback. To ensure the reproduction of the correct stability behavior for the stable LP3, the flame response has been excluded from the corresponding simulation.
Regarding boundary conditions, the inlet is treated as energy-neutral and the outlet as non-reflective, while all walls are modeled as sound-reflecting. The simulations have been conducted at a constant physical time step of $dt = 1 \cdot 10^{-7}\ s$. To excite the chamber acoustics, a pressure disturbance initial condition is set eccentrically in the front chamber section.

5. Results

In this section, the current status of the three groups working towards a reliable procedure for the extraction and comparison of damping rates is presented. On the experimental side, slightly different versions of the parameter extraction method described in section 2.3 have been applied to the data. Numerically, the stable LP3 and the unstable LP4 have been studied. Exponential and, for LP3, Lorentzian fitting have been applied, varying several of the parameters described above to yield the robustness of the approaches.

5.1. *Experimental Evaluation*

For the application of the Fokker-Planck method to transverse combustor modes, a validation of the approach has been conducted first. Then, the parameter extraction is evaluated for the four load points, yielding different levels of applicability. In addition, the slightly modified approach used by the DLR has been applied to a load point similar to LP1 and the extracted parameters are compared to results obtained from Lorentzian fitting.

5.1.1. *Validation with Synthetic Signals*

Before applying the new code to experimental data, a validation was performed on synthetic signals, with known parameters. Equations (2.5)-(2.6) are implemented in a Simulink model. It provides time signals $\eta_a(t)$, $\eta_b(t)$ whose envelopes $A(t)$, $B(t)$ and phase difference $\phi(t)$ are extracted with the Hilbert transform. The range of parameters was chosen so as to reproduce qualitative characteristics of experimental data.
Preliminary results give a fair agreement between identified and actual parameters, showing the effectiveness of the method. In order to gain knowledge on the influence of the pre-processing on the parameter identification, several sensitivity studies were conducted on the synthetic signals. Some examples are the study of the influence of filter bandwidth, or the range of examined amplitudes and time delays, or the function adopted for the extrapolation to $\tau = 0$. Other parameters, such as the signal sample frequency, were found to influence the identification process.

5.1.2. *Application to BKD Data*

The developed parameter identification method was finally applied to the BKD experimental data. In particular, the points LP1 to LP4 were analysed. From the available 8 microphone signals, modal amplitudes $\eta_a(t)$, $\eta_b(t)$ are reconstructed with a multi-microphone method. Since in these signals many modes coexist, a bandpass filter was applied around the one of interest. Like in the case of synthetic signals, different filter sizes and other pre-processing parameters were adopted. The aim is in this case to verify if the identification converges to a certain value for some range of pre-processing parameters. The identified parameters were then injected in the Simulink model, and the generated signals compared with the experimental data to check a posteriori the accuracy of the parameter identification. The process is illustrated with LP2 in figure 5.

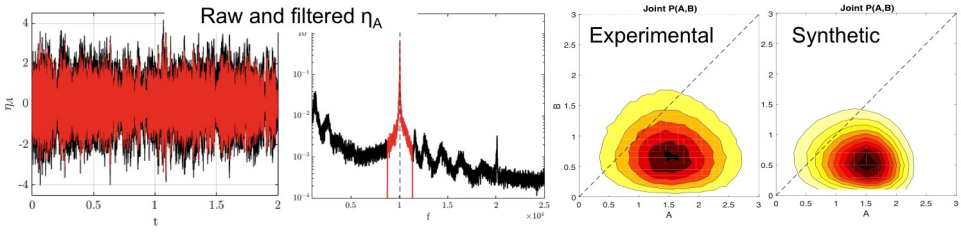

FIGURE 5. Evaluation of LP2. From left to right: acoustic modal amplitude $\eta_a(t)$ before and after band-pass filtering; frequency spectrum; and stationary joint PDFs $P(A, B)$ from experimental measurements and from synthetic signals simulated a posteriori with the identified parameters.

From the analysis of the load points, the following results were obtained:

LP1: The main mode is not clearly isolated: the significant spectrum spans over a broad range of frequency. The system is linearly stable in this point;
Despite that, a fairly stable identification was obtained ($\nu_a \simeq \nu_b \simeq -200$ rad/s);

LP2: Study on the influence of filter bandwidth and examined amplitudes range. Convergence was observed for a certain range ($(\nu_a, \nu_b) \simeq (+110, -150)$ rad/s);
The synthetic replica presents very similar dynamics and statistics;

LP3: The system is unstable, but the spectrum features three peaks within $0.1 f_0$. Therefore, no robust identification is possible;

LP4: Well-isolated peak, highly unstable point;
Peculiar phase statistics (peaks at 0 and $-3\pi/4$). Almost standing mode;

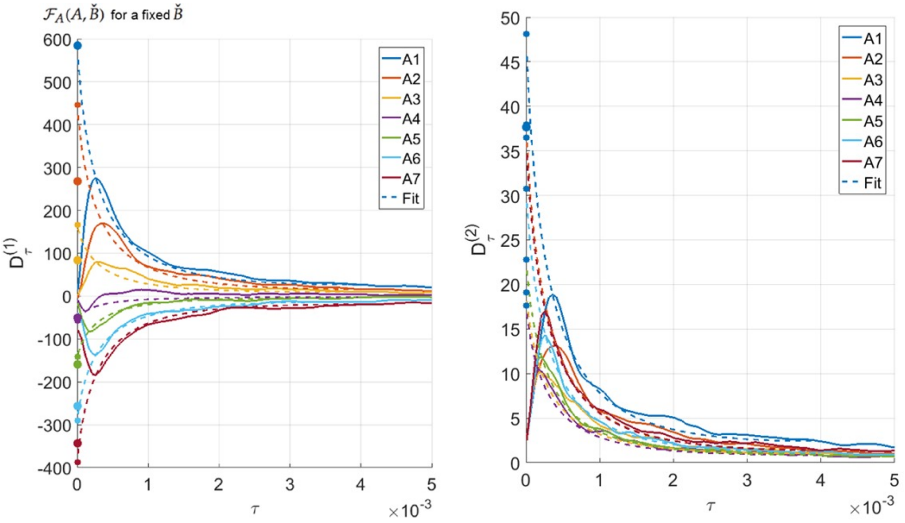

FIGURE 6. First (left) and second (right) transition moments for different amplitudes of $\check{A}$ at the modal value of $\check{B}$; large dots: results from Lorentzian fitting; small dots: extrapolated values

Quite robust identification, but the synthetic replica does not reproduce the same dynamics, especially in terms of phase (the synthetic features two peaks at $\pm\pi/2$).

As described in section 2.3, an alternate extrapolation approach has been used for the Fokker Planck method as well. It has been applied to a stable load point similar to LP1, but with significantly less interference from neighbouring modes. This allows for a direct comparison of the predictions by the Fokker Planck method to the results of a Lorentzian fit, which can be used in this case to precisely extract the parameters of interest. Since extrapolations used to obtain the limits to zero of the probability transition moments are carried out for a single value of the modified envelope amplitude of the orthogonal mode $\check{B}$ (cf. section 2.3.1), the results can be clearly shown for selected amplitudes of the A mode. The first and second transition moment computations are shown in figure 6 along with optimized fits used to capture the limit to zero behavior of these moments. The corresponding values of the A mode are given in figure 7. The results of the application of the Fokker Planck parameter extraction method to the A mode are compared with those obtained with the Lorentzian fit in table 1. The second transition moment computations under-predict the noise intensity by 19% if an average of the extrapolated values is taken. This may be due to the presence of neighboring modes in the analysis. Both Γ_a and ν_a can be obtained by matching the analytical expression of the drift coefficient to the extrapolated value of the first transition moment for each considered amplitude. An optimization over all the amplitudes over-predicts Γ_a by 14%, and over-predicts the absolute value of the growth rate by 8%.

5.2. *Numerical Results*

The numerical computations show a clear, standing first transverse mode for both cases. The mode orientation is determined by the location of the initial excitation. Correspondingly, no mode decomposition is necessary for the damping rate extraction. The evaluated signal is taken at one of the pressure anti-nodes, close to the faceplate. In the following, damping rates are computed for the stable LP3, whereby the influence of the

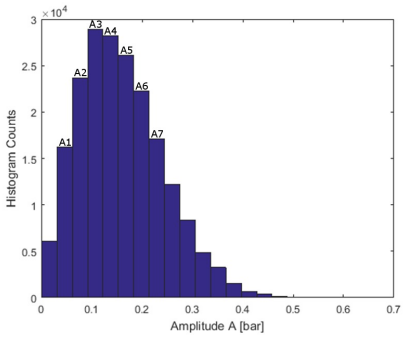

FIGURE 7. Histogram of amplitudes

TABLE 1. Results

Method	Noise Intensity, $bar^2 s^{-4}/Hz$	Growth Rate, rad/s
Lorentzian	$1.35 \cdot 10^{12}$	-2124
Average	$1.09 \cdot 10^{1}2$	-
Optimized	$1.54 \cdot 10^{1}2$	-2287

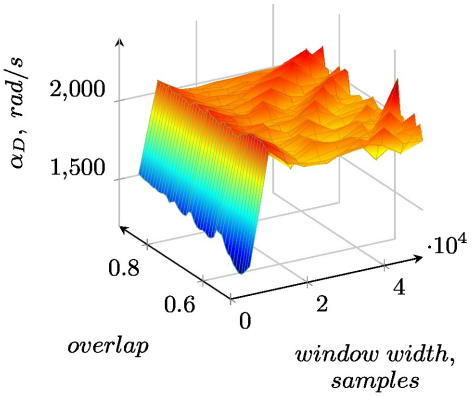

FIGURE 8. Damping rates obtained for LP3 from short time FFT via exponential fitting

TABLE 2. Damping rates for LP3

Exponential, rad/s	Lorentzian, rad/s
$1839 - 2232$	$1991 - 1998$

extraction parameters is studied. Subsequently, the unstable load point LP4 is examined using exponential fitting.

5.2.1. *LP3*

Since LP3 is stable both, exponential and Lorentzian fitting can be applied to this load point. The results of the former are shown in figure 8 for different window sizes and relative overlap. The most significant influence is observed for the window width. This can be explained via the associated frequency resolution. At low window widths, the spectrum is not resolved fine enough to extract the signal content at the desired eigenfrequency with sufficient accuracy. With increasing window width and thus frequency resolution, a plateau is reached. Here, the damping rates still shows a dependency on the windowing parameters, however it is much smaller than observed at low window widths. The dependence of the damping rate on the overlap is comparable to the fluctuations occurring at this plateau, showing no distinct trend. The range of calculated damping rates at the plateau is given in table 2 A considerable range of the extracted damping rates is visible. A possible factor playing a role for this behavior is the loss of temporal resolution at high window widths.

Results of the Lorentzian fit with different frequency ranges considered are shown along with fitted profiles in figure 9. The distortion of the PSD from its ideal shape by

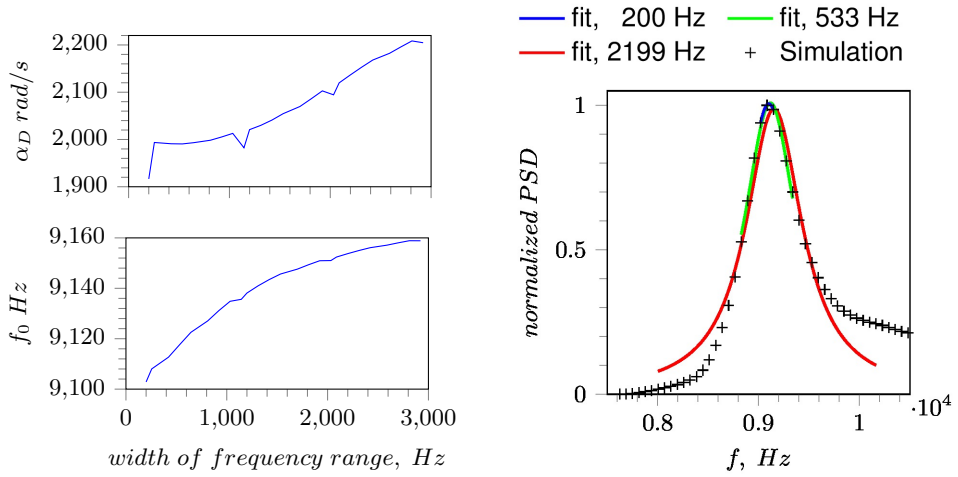

FIGURE 9. Damping rates and eigenfrequencies (left) for LP03, obtained from Lorentzian fitting and fitted profiles (right)

neighboring modes is clearly visible. This affects the extracted damping rates as well (figure 9 (left)). At wide frequency ranges a distinct dependence of the damping rates on the fitting frequencies is visible. Likewise, at the lowest considered frequency range, a sudden decrease in the computed damping rate is visible, related to the low number of data points available for fitting. However, in the range between about $250\ Hz$ and $800\ Hz$ a plateau forms, where the damping rate only weakly varies with frequency range, indicating an appropriate choice for damping rate extraction. The respective values are given in table 2. Regarding the frequency range, this method yields robust identification. Compared to the results obtained from exponential fitting, the damping rates from the Lorentzian fits are contained within the range predicted by the exponential approach.

5.2.2. *LP4*

The damping rates extracted via short time FFT from LP4 are shown in figure 10 (left). Strong growth rates are predicted, which are probably overestimated due to the simple feedback model used. Unlike for LP3, no distinct dependence on the window width is visible. However, at a size of about $20000\ samples$, several strong minima and maxima occur at various values of overlap. This indicates that the damping rate should be evaluated for longer windows, where a smaller variation with window size is present. A comparison with results for the same case without flame feedback (figure 10 (right)) shows that for the then stable configuration the same characteristic behavior as for LP3 is obtained. Transition to the plateau value occurs at about the same window width as the strong extrema for the unstable cases.

6. Conclusion

Damping rates have been extracted from experimental and numerical pressure data of a rocket combustion chamber using Lorentzian and Exponential fitting as well as Fokker-Planck parameter extraction. Numerical data were obtained from the solution of the Linearized Euler Equation, resulting in different signal characteristics compared to

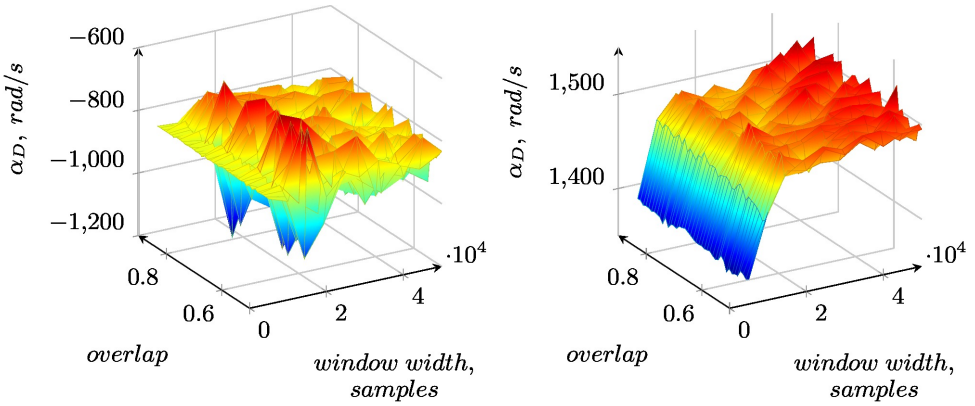

FIGURE 10. LP4 damping rates from exponential fitting; with (left) and without flame feedback (right)

the experiment.

The evaluation of experimental results using the Fokker-Planck approach revealed a dependence of the applicability of this method on the load point under consideration. For the stable LP1 growth rates of about $-200\ rad/s$ were identified and for LP2 $+110\ rad/s$ as well as $-150\ rad/s$ for the respective modal contributions. The evaluation of the additional load points will require further considerations. Parameter extraction for a load point similar to LP1, evaluated with a different extrapolation method indicates stronger damping with a growth rate of about $-2287\ rad/s$ and similar results when using the Lorentzian fit. The reasons for the discrepancy between the different extraction methods need to be studied further.

Numerically, LP3 and LP4 have been studied. It has been found that for the stable load points, the Lorentzian fit yields more robust results compared to the exponential fitting. The latter showed a significant influence of the window width, whereby a lower limit of this parameter could be identified. For the unstable LP4, strong damping rates were calculated, which is probably related to an overprediction of the simple flame model included in the simulation.

Altogether, the results from Lorentzian and exponential fitting were in the same range, indicating their principle applicability with further work needed for the robustness of the latter. Likewise, some promising results were achieved, showing the potentiality of the Fokker-Planck method. However, some of the analysed points cannot be processed with the current tool and need further consideration.

Acknowledgments

Financial support has been provided by the German Research Foundation (Deutsche Forschungsgemeinschaft – DFG) in the framework of the Sonderforschungsbereich Transregio 40.

References

[1] BRONSTEIN, I.N. AND SEMENDJAJEW, K.A. (1991). *Taschenbuch der Mathematik*. B. G. Teubner Verlagsgesellschaft Stuttgart/Leipzig und Nauka Verlag Moskau.

[2] NOIRAY, N. AND SCHUERMANS, B. (2013). Deterministic Quantities Characterizing Noise Driven Hopf Bifurcations in Gas Turbine Combustors. *International Journal of Non-Linear Mechanics*, **50**, 152–163. DOI 10.1016/j.ijnonlinmec.2012.11.008.

[3] Test Case HF-7: LOX/H2-Combustion with Self-Sustained Acoustic Excitation.

[4] GRÖNING, S., SUSLOV, D., OSCHWALD, M. AND SATTELMAYER, T. (2013). Stability Behaviour of a Cylindrical Rocket Engine Combustion Chamber Operated with Liquid Hydrogen and Liquid Oxygen. In: *5th European Conference for Aeronautics and Space Sciences EUCASS 2013*. URL `http://elib.dlr.de/85311/`.

[5] SCHULZE, M. (2016). *Linear Stability Assessment of Cryogenic Rocket Engines*. Ph.D. thesis, Technische Universität München. URL `www.td.mw.tum.de/fileadmin/w00bso/www/Forschung/Dissertationen/schulze16.pdf`.